Desalination and Water Treatment
www.deswater.com
doi: 10.1080/19443994.2014.972984

57 (2016) 900–907
January

Taylor & Francis
Taylor & Francis Group

Visible light induced photocatalytic decolourisation of rhodamine B by magnetite nanoparticles synthesised using recovered iron from waste iron ore tailing

S.K. Giri[a,b], N.N. Das[b,*]

[a]*Department of Chemistry, Utkal University, Bhubaneswar 751 004, Orissa, India*
[b]*Department of Chemistry, North Orissa University, Baripada 757 003, Orissa, India, Tel. +91 6792 252088; Fax: +91 6792 253908; emails: dasnn64@rediffmail.com, chemnou@gmail.com (N.N. Das)*

Received 22 February 2014; Accepted 21 September 2014

ABSTRACT

The photocatalytic activity of highly dispersed magnetite nanoparticles (MNP), synthesised using ferric iron recovered from waste iron ore tailing and reagent grade ferrous chloride by coprecipitation, for the decolourisation of rhodamine B (RhB) under visible light (VL)/sunlight was evaluated. The effects of different reaction parameters such as pH, dye concentration, catalyst dose and externally added H_2O_2 were also investigated. MNP with sizes in the range 8–23 nm and relatively low band gap (1.67 eV) showed good photocatalytic activity, magnetic separability and stability for repeated use. More than 85% of RhB (10 mg/l) is found to be decolourised within 2 h under VL with a MNP dose of 0.51 g/l. Suitable mechanisms have been proposed to account the photocatalytic activities in the presence and absence of H_2O_2. Results obtained in the current study may be useful to prepare suitable photocatalyst combinations with other semiconducting materials for photocatalytic remediation of different water contaminants including organic dyes.

Keywords: Iron ore tailings; Magnetite nanoparticles; Nanophotocatalyst; Rhodamine B; Decolourisation

1. Introduction

Organic dyes are one among the most extensively used colouring agents in textile, pharmaceuticals, cosmetic and paper industries [1]. Due to their extensive use and substantial loss (*ca*. 10–15%) during the manufacturing and dyeing processes, the effluents containing dyes are highly coloured and are considered as potential source of water pollution [1–3]. These effluents produce adverse effects on the environment due to their nonbiodegradability, toxicity, potential carcinogenic and mutagenic nature. Rhodamine B (RhB), a commonly used basic dye with xanthene moiety (Fig. 1), has many toxic effects such as irritation to the skin, eyes, gastrointestinal and respiratory tracts and is also believed to be carcinogenic. Despite the ban on its use in foods and cosmetics, RhB is still extensively used in dyeing and staining processes [4–6]. Treatment of effluents containing RhB is therefore essential before their final discharge to the environment. A variety of physical, chemical and biological based methods have been studied/adopted in practice for removal of RhB from its effluents [7–10]. In addition, the photocatalytic and sonochemical

*Corresponding author.

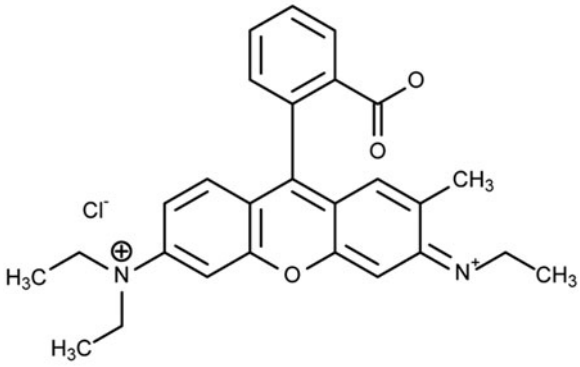

Fig. 1. Structure of rhodamine B (RhB).

decolourisation/ degradation of RhB have also been successfully demonstrated as promising methods for its remediation [11–17]. The photocatalytic decolourisation/degradation of RhB has several advantages over other processes especially in terms of the cost and generation of secondary wastes [18–20]. In this regard, a photocatalytic system active under visible/ sunlight (SL) would be ideal for its large scale practical applications. The wide band gap (3.0–3.2 eV) and low activity of under visible light (VL)/SL limits the use of neat TiO_2 photocatalyst in the treatment of actual dye-contaminated water [18,19]. Although doping of metals or nonmetals in neat TiO_2 lowers the band gap and increases the VL activity, the separation of suspended photocatalysts from the treated water is another major problem in recycling the catalysts for reuse [18–22]. Hence, the development of an easy and effective method to separate the photocatalyst from the treated water is a prerequisite for its practical application to waste water treatment. In the past few years, various magnetic photocatalysts have been developed using the concept of core-shell type of structure (e.g. Fe_3O_4/TiO_2) where magnetic and semiconducting materials are used as a core and shell, respectively [13,23–26]. The Fe_3O_4/TiO_2 photocatalyst has been not only found active under VL but also separated easily by applying external magnetic field. As the overall activity of Fe_3O_4/TiO_2 photocatalyst is partly dependent on the properties of Fe_3O_4, an assessment on the activity and stability of Fe_3O_4 alone is desirable.

Keeping the above in view and in sequel to the previous studies on the utilization of waste iron ore tailing (IOT) for value added materials [27,28], the present study aimed to evaluate the photocatalytic efficiency of magnetite nanoparticles (MNP) synthesized using waste IOT as one of the starting materials. The decolourisation of a model dye (RhB) under VL/ SL at varying conditions was studied in this work.

2. Experimental

2.1. Materials

IOT, used as the ferric source for synthesis of MNP, primarily constitutes of Fe, Si and Al (Fe_2O_3, 55.78; SiO_2, 16.58; Al_2O_3, 15.46; P_2O_5, 1.61; CaO, 1.44; MgO, 0.13; LOI, 9.01 wt.%) with goethite, hematite and magnetite as the main iron bearing phases [27]. RhB (BDH) and H_2O_2 (30%, Merck) were used as received for photocatalytic experiments. All other chemicals and reagents used were of analytical grade.

2.2. Synthesis and characterization of MNP

MNP was synthesised by coprecipitation of a mixture of recovered ferric iron from IOT and $FeCl_2{\cdot}4H_2O$ by liquid ammonia under N_2 atmosphere as described earlier [27]. Powder XRD patterns were recorded on a Rigaku Miniflex II using CuK_α radiation at scanning speed 1.2° min^{-1}. FT-IR spectra in KBr phase were taken on a Nicolet (Impact I-410) FT-IR spectrometer averaging 32 scans at a resolution of 4 cm^{-1}. Magnetic measurements were done by a vibrating sample magnetometer (Lakeshore 7410) at room temperature in the range +20,000 to −20,000 G. The size and distribution of MNP were studied by transmission electron microscope (FEI, TECHNI, B^2 20, TWIN) operated at 200 kV. UV–visible–diffuse reflectance spectra (UV–vis–DRS) of MNP was recorded on a Shimadzu, UV-2400 spectrophotometer using $BaSO_4$ as reference. The point of zero charge (pH_{pzc}) of MNP was determined by batch acid–base titration as follows. A definite amount of MNP was added to 50 ml of 0.01 M KCl solution (solid-to-liquid ratio ~1:100) taken in 100 ml beaker. The initial pH of the solution was recorded. Then, 0.01 M HCl or 0.01 M NaOH was added to the slurry in 0.1 ml increment with continuous stirring, and the pH was measured after the addition of each increment. The addition of HCl or NaOH was continued till the pH value was reached to ~3.0 or 10.0, respectively. Finally, the volume of HCl or NaOH added was plotted against the pH values recorded. The point at which the pH value was crossed the ordinate was taken as the point of zero charge of MNP.

2.3. Photocatalytic activity

The photocatalytic activity of MNP was evaluated for the decolourisation of rhodamine B (Fig. 1) under VL and SL. Photocatalytic experiments in air were carried out in a double walled 250 ml capacity three

necked glass reactor fitted with 125 W high pressure Hg lamp as the light source. The lamp was equipped with a cut-off filter to remove any radiation <450 nm and to ensure irradiation only by VL. All the experiments were performed at constant temperature and under mechanical stirring condition. A certain amount of MNP (0.085–1.20 g/l), dispersed into 100 ml of RhB solution (5.0–40.0 mg/l), was adjusted to desired pH and was allowed to attain the equilibrium for 20 min in dark before irradiation with either visible or SL. For solar light decolourisation, a 100-ml conical flask containing RhB and MNP at desired pH was placed under direct SL in the University campus (21˚56´ N 86˚43´). All experiments were performed under clear sky condition between 11.00 am and 3.00 pm during summer season (April–June) with stirring. At regular intervals or the end of reaction, a definite portion of reactant solution was withdrawn, magnetically treated to separate the MNP and the concentration of residual RhB in the supernatant was computed from the absorbance values at 545 nm. The efficiency of decolourisation was evaluated from the following Eq. (1):

$$P\,(\%) = (C_0 - C_t)/C_0 \times 100 \quad (1)$$

where P is the % of decolourisation, C_0 and C_t are the RhB concentrations (mg/l) at the beginning and time, t, respectively. The reproducibility of all photocatalytic experiments was checked by repeating the measurements at least twice and was found to be within the acceptable limit (±5%).

3. Results and discussion

3.1. Characterizations of MNP

The chemical analyses for total Fe, Fe(II) and other trace metals show the purity of synthesised MNP. PXRD pattern and FT-IR spectra of MNP with characteristic diffraction peaks and absorption bands further indicate the formation of well crystalline single phase MNP [27]. The saturation magnetization (σ_s) value (35.7 emu/g) is comparable with the values reported for MNP but relatively lower than that of bulk magnetite (σ_s = 92 emu/g) [27]. The TEM micrographs showed that the MNPs are mostly spheroidal or cubic in shape with diameters in the 8.3–23.0 nm range.

The band gap energy and extent of interaction of substrate with the photocatalyst are two important parameters among others, which ultimately decide the overall photocatalytic activity. In order to correlate these properties of MNP with activity, the band gap energy and point of zero charge (pH_{pzc}) of MNP were determined. The UV–vis–DRS of MNP, presented in

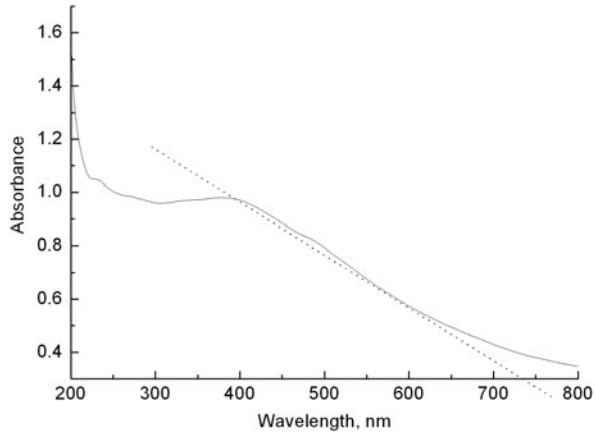

Fig. 2. UV–visible–DRS of vacuum dried neat MNP.

Fig. 2, shows significant absorption of light at higher wavelength side indicating its possible photocatalytic activity under VL irradiation. The estimated band gap energy of MNP (1.67 eV) is much higher than the value of bulk magnetite (~0.1 eV) but relatively lower than TiO_2 (~3.2 eV) [19]. MNP is an amphoteric solid can develop positive and negative charges, respectively, due to protonation as ($FeOH + H^+ \rightarrow FeOH_2^+$) and deprotonation ($FeOH \rightarrow FeO^{-+}H^+$) of FeOH sites generated on surface of magnetite when dispersed in water. The pH_{pzc} value of MNP (7.1 as evident from Fig. 3) compares well with those reported previously for MNPs [27,28]. Accordingly, the surface of MNP will be either positively or negatively charged at pH <7.1 or >7.1, respectively. Due to the variation of

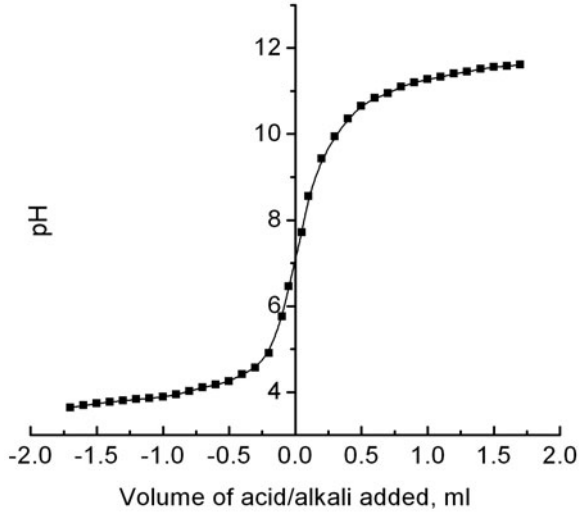

Fig. 3. Determination of point of zero charge of MNP by acid–base titration.

surface charge with pH, MNP has the advantage of interacting both anionic and cationic dyes from water to facilitate their photocatalytic decolourisation.

3.2. Photocatalytic activity

The time course photocatalytic decolourisation of RhB by MNP at pH ~7.5, under both VL and SL, are presented in Fig. 4. The corresponding absorption spectra of RhB solution at different times during VL irradiation is also shown in Fig. 4 (inset). It is seen that the absorption maximum (λ_{max}) steadily decreases upon irradiation, without any observable shift in the peak positions indicating the degradation of RhB is primarily due to the decomposition of conjugated chromophore structure rather than de-ethylation process [23,29]. De-ethylation of rhodamine B leads to the formation of rhodamine with an observable shift of absorption maxima to 497 nm [15]. The following observations show the photocatalytic effect of MNP. The spectral change of RhB in the absence of MNP is negligible indicating the decolourisation of aqueous RhB takes places primarily through photocatalysis. A relatively less amount of initial dark adsorption of RhB on MNP (~5%) further indicates the photocatalytic effect of MNP. Under identical conditions, the activity of MNP under VL is also found significantly higher than that under SL throughout the reaction period. For instance, it is evident from Fig. 4 that more than 86% of RhB (initial concentration, 10 mg/l) is decolourised within 120 min under VL irradiation (curve 3) compare to only 32% under SL (curve 4). It is also seen that initial photo-decolourisation up to 120 min is relatively fast followed by slow process up to 240 min. Hence, all further experiments to evaluate the photocatalytic efficiency of MNP under varying conditions and the apparent rate constants were carried out keeping the reaction time fixed at 120 min.

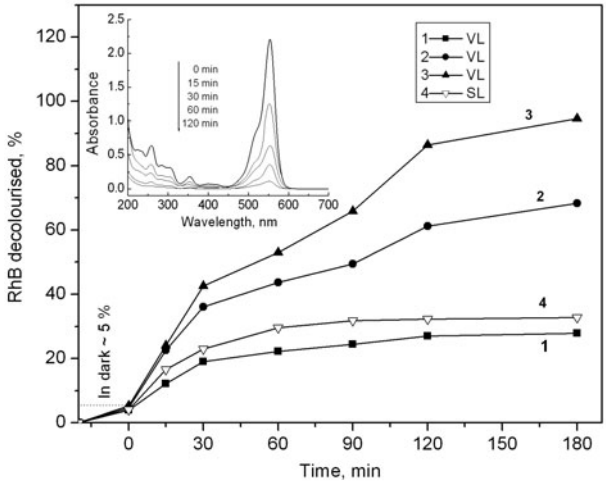

Fig. 4. Effect of contact time on decolourisation of RhB (10.0 mg/l) by MNP at pH ~7.5 ± 0.2 under VL and SL. (1), (2) and (3) represent the activity under VL with MNP dose of 0.085, 0.255 and 0.51 g/l, respectively, while (4) represents the activity under SL with MNP dose of 0.51 g/l. (Inset) Time course spectral scan of RhB (10 mg/l) under VL with MNP dose of 0.51 g/l.

The pH of the reactant solution is an important parameter affecting the overall adsorption/photocatalytic decolourisation of dyes by oxide-based photocatalysts. The pH of the solution may change: (1) the surface charge of the adsorbent, (2) the degree of ionization of the adsorbate molecule and (3) extent of dissociation of functional groups, if any. In order to avoid the last two effects leading to variable adsorption of RhB on MNP surface, the photocatalytic decolourisation was carried out at pH values (~5.0–12.0) above the acid dissociation constant of RhB (pK_a = 3.7) where it mostly exists in zwitterionic form due to deprotonation of carboxyl group [19]. The results of the RhB decolourisation at varying pH along with its adsorption on MNP at the same pH values are presented in Fig. 5. It is seen that the adsorption of RhB is progressively decreased (not shown) with the increase of pH, reached a minimum value at pH ~8.0 and then increased on further increase of pH. The decrease of adsorption at pH > 5.0 is presumably due to aggregation of zwitterions form of RhB leading to bigger molecular form (dimer) while at higher pH values, a decrease in aggregation of RhB is expected as OH^- starts competing with the interaction between $-N^+$ (xanthene moiety) and COO^- group causing an

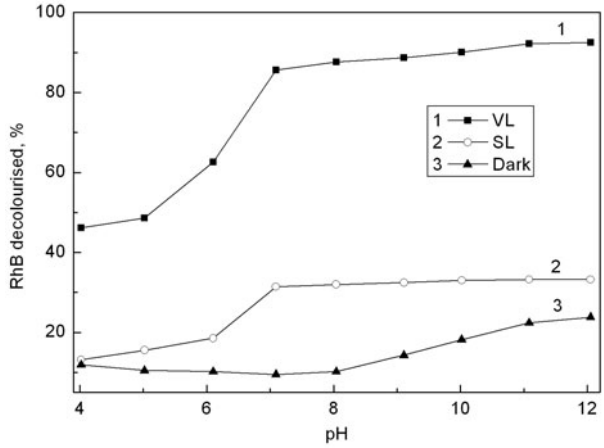

Fig. 5. Effect of pH on decolourisation of RhB under VL (1) and SL (2). (RhB, 10 mg/l; MNP, 0.51 g/l; contact time, 2 h).

increase of RhB adsorption. On the other hand, the decolourisation of RhB due to photocatalysis is almost linearly increased with the increase of pH from ~5.0 to 7.0, and thereafter, only marginal increase is observed on further increase of pH. The increase in dye decolourisation/degradation with the increase of pH, due to facile interaction between the dye molecules and the photocatalysts, has been reported earlier [19,26,30].

In order to see the effect of catalyst dose, the experiments were performed by varying the catalyst amount from 0.085 to 1.2 g/l at fixed pH (7.5 ± 0.2) and initial RhB concentration (10 mg/l), and the results obtained are depicted in Fig. 6. As evident, the decolourisation of dye is increased almost linearly with the increase of MNP dose up to 0.51 g/l, primarily due to availability of greater amount of active sites on the catalyst surface. On further increase of MNP dose, the activity is not linearly increased with the amount of MNP presumably due to aggregation of MNP which in turn reduces the number of active sites for photo-decolourisation. The other factor of decreased activity could be due to the increased turbidity of reactant solution with the increase of catalyst dose resulting in a decrease of VL penetration in to the reactant solution [29,30].

The concentration of dye is another important factor which influences its overall adsorption/decolourisation by the photocatalyst. The effect of RhB concentration in the range 5.0–40.0 mg/l is depicted in Fig. 7. Although the percentage of decolourisation is progressively decreased with the increase of RhB concentrations, the amount of RhB decolourisation is increased from 9.6 to 36.6 mg of RhB/g of MNP and 4.0–9.1 mg of RhB/g of MNP under VL and SL,

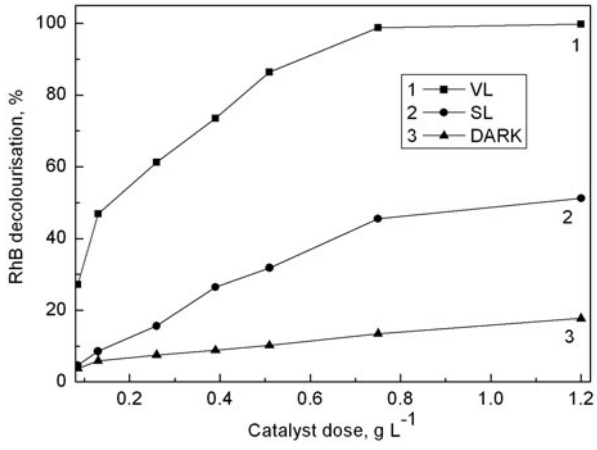

Fig. 6. Effect of MNP dose (0.085–1.20 g/l) on decolourisation of RhB (10 mg/l) at pH ~7.5 ± 0.2.

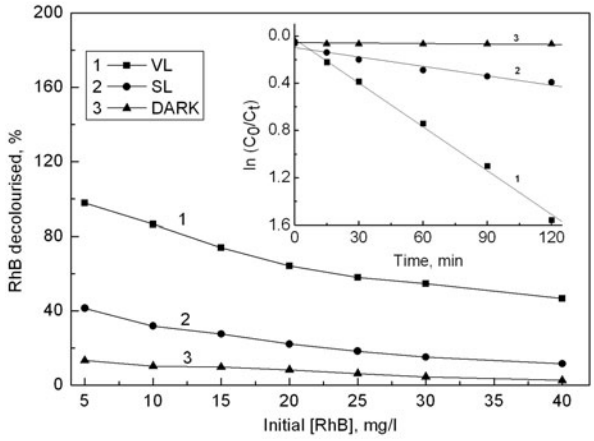

Fig. 7. Effect of initial concentration (5–40 mg/l) on RhB decolourisation at pH ~7.5 under VL (1) and SL (2) (MNP, 0.51 g/l). (Inset) Fitting of RhB decolourisation data to first-order kinetics.

respectively. Further, the decolourisation data up to 120 min are found to follow the first-order kinetics (Eq. (2)):

$$\ln (C_0/C_t) = kt \quad (2)$$

where C_0 and C_t are the concentrations of RhB at the beginning and time t, respectively, and k is the rate constant. The representative plots of ln (C_0/C_t) vs. t are presented in Fig. 7 (inset). The first-order rate constants, derived from linear plots of ln (C_0/C_t) vs. time are found to be 1.89, 0.997,0.52, 0.40 and 0.31 h^{-1} for initial concentrations of 5, 10, 20, 30 and 40 mg/l, respectively, under VL irradiation. As expected, much lower values of rate constants (0.267, 0.192, 0.125, 0.082 and 0.061 h^{-1}) are obtained under SL with the same concentrations of RhB. The values of rate constant are significantly decreased with the increase of initial RhB concentration at least at lower concentrations (≤10 mg/l), but there is marginal decrease at higher concentrations. Table 1 presents a comparative photo-decolourisation activity of MNP and other photocatalytic systems. It is worth noting that MNP exhibits comparable or better activity than other catalysts even under VL and may be exploited further for its possible use in real systems alone or in combination with suitable semiconductor supports.

On the basis of experimental observations and earlier reports [11–15,31], the photocatalytic decolourisation without H_2O_2 occurs most likely either through (i) photoexcitation of Fe_3O_4 leading to the electron/hole pairs on its surface followed by the formation of

Table 1
Comparative RhB decolourisation in aqueous medium under different light sources using various photocatalytic systems

Photocatalytic systems	Catalyst dose (g/l)	RhB (mg/l)	pH	Reaction time (min)	Light source	Decolourisation (%)	Ref.
$LaCoO_3$ nanofibers	0.50	100	4.0	60	UV	30.0	[11]
Mesoporous α-Fe_2O_3	0.50	4.79	–	135	UV	84.9	[12]
Ag/Fe_3O_4/SiO_2	0.5	25	–	150	k > 420 nm	10	[13]
Eu^{3+}- doped $ZnWO_4$	1.00	4.79	–	100	UV	~90.0	[29]
$ZnFe_2O_4$ nanoparticles	0.80	20	–	300	200–700 nm	38.4	[34]
$ZnFe_2O_4$ nanosphere	0.80	20	–	300	200–700 nm	100	[34]
ZnO nanocrystals	1.00	24.0	–	90	UV	99.9	[35]
BiOCl/$H_4SiW_{12}O_{40}^{4-}$	0.0575	9.58	2.5	300	VL	95.0	[36]
MNP	0.51	5.0	7.5	120	VL	97.7	This work
MNP	0.51	10.0	7.5	120	VL	86.4	This work
MNP	0.51	20.0	7.5	120	VL	64.3	This work
MNP	0.51	25.0	7.5	120	VL	58.0	This work
MNP + H_2O_2	0.51	10.0	12.0	120	VL	92.5	This work
MNP	0.51	5.0	7.5	120	SL	41.4	This work
MNP	0.51	10.0	7.5	120	SL	31.8	This work
MNP	0.51	20.0	7.5	120	VL	22.3	This work
MNP	0.51	25.0	7.5	120	VL	18.1	This work
MNP + H_2O_2	0.51	10.0	12.0	120	SL	33.2	This work

hydroxide radical ($HO^{\bullet}$) by the decomposition of the water or by reaction of the holes with HO^- and its reaction with RhB to yield the degradation products is delineated in Eqs. (3)–(6).

$$Fe_3O_4 + h\nu \rightarrow Fe_3O_4(e^-_{CB} + h^+_{\nu B}) \quad (3)$$

$$H_2O + h^+_{\nu B} \rightarrow H^+ + OH^{\bullet} \quad (4)$$

$$HO^- + h^+_{\nu B} \rightarrow HO^{\bullet} \quad (5)$$

$$HO^{\bullet} + RhB \rightarrow \text{degradation products} \quad (6)$$

and/or (ii) absorption of VL Fe_3O_4/RhB system leading to the excitation of the surface-adsorbed dye molecule (Eq. (7)), which affects the charge transition into the conduction band of Fe_3O_4 in the excited state (Eq. (8)). The electron in the conduction band (e^-_{CB}) is then transferred to molecular oxygen, leading to the formation of a series of radicals capable of decolourising/degrading RhB.

$$Fe_3O_4/RhB + h\nu \rightarrow Fe_3O_4/RhB^* \quad (7)$$

$$Fe_3O_4/RhB^* \rightarrow Fe_3O_4(e^-_{CB})/\ RhB^+ \quad (8)$$

$$Fe_3O_4(e^-_{CB}) + O_2 \rightarrow Fe_3O_4 + O_2^{-\bullet} \quad (9)$$

$$H_2O + O_2^{-\bullet} \rightarrow HOO^{\bullet} \quad (10)$$

$$2\ HOO^{\bullet} \rightarrow O_2 + H_2O_2 \quad (11)$$

$$HOO^{\bullet} + H_2O + e^-_{CB} \rightarrow H_2O_2 + OH^- \quad (12)$$

$$H_2O_2 + e^-_{CB} \rightarrow HO^{\bullet} + OH^- \quad (13)$$

$$H_2O_2 + O_2^{-\bullet} \rightarrow HO^{\bullet} + OH^- + O_2 \quad (14)$$

$$HO^{\bullet}/O_2^{-\bullet} + RhB \rightarrow \text{degradation products} \quad (15)$$

One of the products of photocatalytic degradation of organic pollutants in water is H_2O_2 which itself can act as a source of active free radicals. Also, the addition of H_2O_2 often accelerates the rate of dyes decolourisation. In order to investigate the effect of H_2O_2, the photocatalytic decolourisation of RhB (20 mg/l) was performed with initially added varying amounts of H_2O_2 (3–30 mM), and the results obtained are shown in Fig. 8 along with those in the presence of MNP or H_2O_2 alone. Control experiment with only H_2O_2 without irradiation shows a very little decolourisation of RhB (3–4%). On irradiation with VL, the RhB decolourisation in the presence of H_2O_2 is significantly enhanced on irradiation and reaches up to 34% in 3 h. A much higher value (70%) of RhB decolourisation

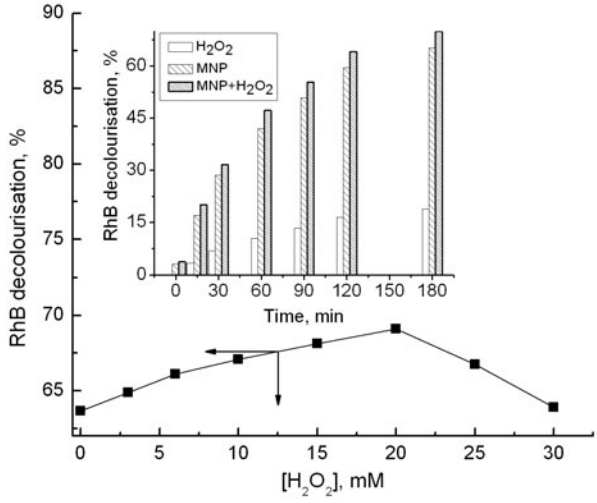

Fig. 8. Effect of H_2O_2 concentration on decolourisation of RhB under VL at pH ~7.5 ([RhB], 20 mg/l; MNP dose, 0.51 g/l). (Inset) Comparative RhB decolourisation by MNP in the presence and absence of H_2O_2.

has been reported in the presence UV/H_2O_2 [32,33]. On the other hand, the addition of H_2O_2 (10 mM) along with MNP marginally increases the RhB decolourisation from that of neat MNP. This increase of decolourisation is primarily attributed to the additional ·OH radicals produced by either through the reduction of H_2O_2 at the conduction band (Eq. (13)) or by the self-decomposition reactions of the molecule. However, the ·OH radical scavenging by H_2O_2 (Eq. (16)) leading to the formation of less reactive hydroperoxyl (·OOH) is one of the main factors for the much lower enhancement of RhB decolourisation in the presence both H_2O_2 and MNP. Further increase of H_2O_2, beyond 20 mM, results a decrease of RhB decolourisation primarily due to interaction between ·OOH and ·OH radicals and also due to self-recombination ·OH radical (Eqs. (17) and (18)).

$$H_2O_2 + HO^{\cdot} \rightarrow H_2O + HOO^{\cdot} \quad (16)$$

$$HOO^{\cdot} + HO^{\cdot} \rightarrow H_2O + O_2 \quad (17)$$

$$HO^{\cdot} + HO^{\cdot} \rightarrow H_2O_2 \quad (18)$$

The reusability of the MNP relies on its stability without losing the activity. In order to see the stability, the catalyst carefully separated by applying magnetic field was subjected with a fresh dye solution (10 mg/l) and irradiated under same light source for 3 h. This process was repeated for two more times. It is seen that the RhB decolourisation in the fourth catalytic run is ~88% as against ~94% in the first cycle. Moreover, the analysis by AAS indicates that there is no detectable Fe in the reactant solution after each catalytic run, indicating MNP is fairly stable under the experimental conditions and can be reused without any significant decrease in the activity.

4. Conclusions

Well crystalline MNP synthesized using waste IOTs as one of the starting materials was found to be an effective photocatalyst for decolourisation of RhB under VL/SL. More than 85% of 10 mg/l RhB was decolourised within 2 h under VL with a catalyst dose of 0.51 g/l. Under identical conditions, but in the absence of visible/SL, only 5–7% of RhB was decolourised primarily due to it adsorption on MNP surface. The rate of RhB decolourisation followed a first-order kinetics which was found to be decreased with the increase of initial dye concentration. More importantly, the magnetite nanophotocatalyst can be easily separated from the reactant solution using an external magnetic field and can be used in cycles without any significant decrease in its activity.

References

[1] C.C.I. Guaratini, M.V.B. Zanoni, Textile dyes, Quim. Nova. 23 (2000) 71–78.
[2] T. Robinson, G. McMullan, R. Marchant, P. Nigam, Remediation of dyes in textile effluent: A critical review on current treatment technologies with a proposed alternative, Bioresour. Technol. 77 (2001) 247–255.
[3] V.K. Gupta, Suhas, Application of low-cost adsorbents for dye removal—A review, J. Environ. Manage. 90 (2009) 2313–2342.
[4] Y. Zhang, W. Shi, D. Feng, H. Ma, Y. Liang, J. Zuo, Application of rhodamine B thiolactone to fluorescence imaging of Hg^{2+} in Arabidopsis thaliana, Sens. Actuators, B 153(2011) (2011) 261265.
[5] Y. Ma, M. Zhou, X. Jin, B. Zhang, H. Chen, N. Guo, Flow-injection chemiluminescence determination of ascorbic acid by use of the cerium(IV)–rhodamine B system, Anal. Chim. Acta. 464 (2002) 289–293.
[6] B.S. Virupaxappa, K.H. Shivaprasad, M.S. Latha, Spectrophotometric method for the determination of artenimol using Rhodamine B, J. Chem. Pharm. Res. 4 (2012) 1822–1826.
[7] K. Shakir, A.F. Elkafrawy, H.F. Ghoneimy, S.G. Elrab Beheir, M. Refaat, Removal of rhodamine B (a basic dye) and thoron (an acidic dye) from dilute aqueous solutions and wastewater simulants by ion flotation, Water Res. 44 (2010) 1449–1461.
[8] M.F. Hou, L. Liao, W.D. Zhang, X.Y. Tang, H.F. Wan, G.C. Yin, Degradation of rhodamine B by Fe(0)-based Fenton process with H_2O_2, Chemosphere 83 (2011) 1279–1283.

[9] P. Nigam, G. Armour, I.M. Banat, D. Singh, R. Marchant, Physical removal of textile dyes from effluents and solid-state fermentation of dye-adsorbed agricultural residues, Bioresour. Technol. 72 (2000) 219–226.
[10] E. Forgacs, T. Cserháti, G. Oros, Removal of synthetic dyes from wastewaters: A review, Environ. Int. 30 (2004) 953–971.
[11] B. Dong, Z. Li, Z. Li, X. Xu, M. Song, W. Zheng, C. Wang, S.S. Al-Deyab, M. El-Newehy, Highly efficient $LaCoO_3$ nanofibers catalysts for photocatalytic degradation of rhodamine B, J. Am. Ceram. Soc. 93 (2010) 3587–3590.
[12] S. Bharathi, D. Nataraj, D. Mangalaraj, Y. Masuda, K. Senthil, K. Yong, Highly mesoporous α-Fe_2O_3 nanostructures: Preparation, characterization and improved photocatalytic performance towards Rhodamine B (RhB), J. Phys. D: Appl. Phys. 43 (2010) 015501, doi: 10.1088/0022-3727/43/1/015501.
[13] J. Guo, B. Ma, A. Yin, K. Fan, W. Dai, Photodegradation of rhodamine B and 4-chlorophenol using plasmonic photocatalyst of Ag–AgI/Fe_3O_4@ SiO_2 magnetic nanoparticle under visible light irradiation, Appl. Catal. B 101 (2011) 580–586.
[14] S. Merouani, O. Hamdaoui, F. Saoudi, M.S. Chiha, Sonochemical degradation of Rhodamine B in aqueous phase: Effects of additives, Chem. Eng. J. 158(3) (2010) 550–557.
[15] R. Qiu, D. Zhang, Y. Mo, L. Song, E. Brewer, X. Huang, Y. Xiong, Photocatalytic activity of polymer-modified ZnO under visible light irradiation, J. Hazard. Mater. 156 (2008) 80–85.
[16] R. Nagaraja, N. Kottam, C.R. Girija, B.M. Nagabhushana, Photocatalytic degradation of Rhodamine B dye under UV/solar light using ZnO nanopowder synthesized by solution combustion route, Powder Technol. 215–216 (2012) 91–97.
[17] R. Jain, M. Mathur, S. Sikarwar, A. Mittal, Removal of the hazardous dye rhodamine B through photocatalytic and adsorption treatments, J. Environ. Manage. 85 (2007) 956–964.
[18] D. Robert, S. Malato, Solar photocatalysis: A clean process for water detoxification, Sci. Total Environ. 291 (2011) 85–97.
[19] M. Kitano, M. Matsuoka, M. Ueshima, M. Anpo, Recent developments in titanium oxide-based photocatalysts, Appl. Catal. A 325 (2007) 1–14.
[20] A.D. Paola, E. García-López, G. Marcì, L. Palmisano, A survey of photocatalytic materials for environmental remediation, J. Hazard. Mater. 211–212 (2012) 3–29.
[21] S.G. Kumar, L.G. Devi, Review on modified TiO_2 photocatalysis under UV/visible light: Selected results and related mechanisms on interfacial charge carrier transfer dynamics, J. Phys. Chem. A 115 (2011) 13211–13241.
[22] U.I. Gaya, A.H. Abdullah, Heterogeneous photocatalytic degradation of organic contaminants over titanium dioxide: A review of fundamentals, progress and problems, J. Photochem. Photobiol., C 9 (2008) 1–12.
[23] D. Beydoun, R. Amal, G.K.C. Low, S. McEvoy, Novel photocatalyst: Titania-coated magnetite. Activity and photodissolution, J. Phys. Chem. B 104 (2000) 4387–4396.
[24] X. Xu, X. Shen, G. Zhu, L. Jing, X. Liu, K. Chen, Magnetically recoverable Bi2WO6-Fe_3O_4 composite photocatalysts: Fabrication and photocatalytic activity, Chem. Eng. J. 200–202 (2012) 52–531.
[25] S. Watson, D. Beydoun, R. Amal, Synthesis of a novel magnetic photocatalyst by direct deposition of nanosized TiO_2 crystals onto a magnetic core, J. Photochem. Photobiol., A 148 (2002) 303–313.
[26] S.K. Giri, N.N. Das, Iron oxide/titania photocatalysts derived from $TiO_2{\cdot}nH_2O$ coated ferric hydr(oxide) precursors: Characterizations and visible light photocatalytic activity, Powder Technol. 239 (2013) 193–198.
[27] S.K. Giri, N.N. Das, G.C. Pradhan, Synthesis and characterization of magnetite nanoparticles using waste iron ore tailings for adsorptive removal of dyes from aqueous solution, Colloids Surf. A 389 (2011) 43–49.
[28] S.K. Giri, N.N. Das, G.C. Pradhan, Magnetite powder and kaolinite derived from waste iron ore tailings for environmental applications, Powder Technol. 214 (2011) 513–518.
[29] T. Dong, Z. Li, Z. Ding, L. Wu, X. Wang, X. Fu, Characterizations and properties of Eu^{3+}-doped $ZnWO_4$ prepared via a facile self-propagating combustion method, Mater. Res. Bull. 43 (2008) 1694–1701.
[30] M.J. Pawar, A.D. Khajone, Photodegradation of malachite green dye over sol–gel synthesized nanocrystalline α-Fe_2O_3, J. Chem. Pharm. Res. 4 (2012) 1880–1884.
[31] R.V. Solomon, I.S. Lydia, J.P. Merlin, P. Venuvanalingam, Enhanced photocatalytic degradation of azo dyes using nano Fe_3O_4, J. Iran. Chem. Soc. 9 (2012) 101–109.
[32] F.H. AlHamedi, M.A. Rauf, S.S. Ashraf, Degradation studies of Rhodamine B in the presence of UV/H_2O_2, Desalination 239 (2009) 159–166.
[33] I.K. Konstantinou, T.A. Albanis, TiO_2-assisted photocatalytic degradation of azo dyes in aqueous solution: Kinetic and mechanistic investigations—A review, Appl. Catal., B 49 (2004) 1–14.
[34] X. Li, Y. Hou, Q. Zhao, L. Wang, A general, one-step and template-free synthesis of sphere-like zinc ferrite nanostructures with enhanced photocatalytic activity for dye degradation, J. Colloid Interface Sci. 358 (2011) 102–108.
[35] J. Chang, E.R. Waclawik, Facet-controlled self-assembly of ZnO nanocrystals by non-hydrolytic aminolysis and their photodegradation activities, CrystEngComm 14 (2012) 4041–4048.
[36] C. Chen, J. Li, W. Zhao, J. Zhao, L. Wan, Y. Xu, Visible light induced photocatalytic reaction of rhodamine B dye via 12-tungstosilicic acid in water, Sci. China, Ser. B 46 (2003) 577–582.